NON-BLIND IMAGE RESTORATION WITH SYMMETRIC GENERALIZED PARETO PRIORS

Xing Mei[⋆†] *Bao-Gang Hu*[†] *Siwei Lyu*[⋆]

[⋆] Computer Science Department, University at Albany, SUNY
[†] NLPR, Institute of Automation, Chinese Academy of Sciences

ABSTRACT

This paper presents a new non-blind image restoration method based on the symmetric generalized Pareto (SGP) prior, which models the heavy-tailed distributions of gradients for natural images. Through experiments we show that the SGP model achieves log likelihood scores comparable to the hyper-Laplacian model when fitted to gradients and other band-pass filter responses. More importantly, when incorporated into a Bayesian MAP framework for non-blind image restoration, the SGP model leads to a closed-form solution for a per-pixel subproblem, which affords computational advantages in comparison with the numerical solutions induced from the hyper-Laplacian model. Experimental results show that our method is comparable to existing methods in restoration quality and processing speed.

Index Terms— Symmetric Generalized Pareto, Half-Quadratic Splitting

1. INTRODUCTION

The visual quality of an image can be degraded by a number of factors during the acquisition process, such as motion blur, focus variation and environmental noise. Mathematically, this degradation process can be described as $\mathbf{y} = \mathbf{x} \otimes \mathbf{k} + \mathbf{n}$, where $\mathbf{x}$ is the original image, $\mathbf{k}$ is the convolution kernel (the point spread function), $\mathbf{n}$ is the additive noise and $\mathbf{y}$ is the observed blurry image. The task of image restoration is to recover $\mathbf{x}$ from the degraded observation $\mathbf{y}$ with known or unknown $\mathbf{k}, \mathbf{n}$ information [1]. We mainly focus on the *non-blind image restoration* problem with a known, spatially invariant kernel $\mathbf{k}$. This problem also turns out to be an essential building block for many *blind restoration* algorithms [2, 3].

The non-blind image restoration problem is inherently ill-posed in the presence of $\mathbf{k}$ and $\mathbf{n}$; therefore, a statistical prior model for the clean image $\mathbf{x}$ is of central importance for restoration quality. Priors based on natural image statistics have proven effective for numerous image processing applications, such as the joint distributions of the neighboring wavelet coefficients [4], Field of Experts [5] and the patch priors from EPLL [6]. One well-founded, widely used prior for image restoration is the marginal distributions of gradients and other band-pass filter responses: these distributions are highly kurtotic with tails heavier than the Gaussian and Laplacian models, which can be well modeled with a hyper-Laplacian model [7, 8, 9] or a scale mixture of Gaussians [10]. By encouraging the marginal statistics of the gradients to match these models, high-quality restoration results have been achieved with a general Bayesian maximum-a-posterior (MAP) framework [11, 12]. However, the corresponding MAP problems become computationally challenging due to the non-smooth objective functions. Recently, several fast schemes have been proposed to solve the hyper-Laplacian based problem by decomposing it into two subproblems with half-quadratic splitting [13, 14]. For one subproblem depending on the hyper-Laplacian prior, a 1D optimization process needs to be performed independently on each pixel. Pre-computed look-up tables or iterative approximations are proposed to accelerated the optimization process [13, 14].

In this paper, we propose a novel non-blind image restoration method, which regularizes the marginal behavior of $\mathbf{x}$'s gradients with a *Symmetric Generalized Pareto* (SGP) model. SGP has recently been studied (under different names) by various researchers in the machine learning community [15, 16, 17]. We fit SGP to the heavy-tailed statistics of image gradients and responses of other band-pass filters, and experimentally show that the fitting results of the SGP model are comparable to the widely used hyper-Laplacian model. More importantly, when used as a probabilistic prior in the Bayesian MAP framework, the SGP model leads to a simple closed-form solution for any valid parameter settings, which is conceptually more favorable than the approximate numerical solutions with the hyper-Laplacian model. We quantitatively evaluate our SGP-based method, the hyper-Laplacian based methods [13, 14] and the classic L1 restoration method [18] with various kernel and noise settings. Experimental results show that our method is comparable to the hyper-Laplacian based methods in restoration image quality with improved processing speed. Our evaluation also shows that the restoration performance of the L1 method, though better for Gaussian kernels, becomes inferior to our method when images are degraded with realistic motion-blur kernels.

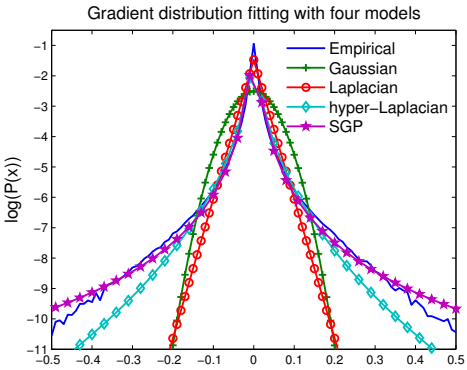

Fig. 1: A typical image gradient distribution (in logarithmic scale) and the fitting results with four parametric models: Gaussian, Laplacian, hyper-Laplacian and SGP.

2. THE SGP MODEL

The Symmetric Generalized Pareto distribution (SGP) is defined by 'symmetrizing' the generalized Pareto distribution [19] to the whole real line as follows:

$$p(x|\omega,\gamma) = \frac{\omega\gamma^{\omega}}{2(|x|+\gamma)^{\omega+1}}, x \in \mathbb{R} \quad (1)$$

where $\omega, \gamma > 0$ are the shape and scale parameters respectively. Large ω values or small γ values lead to sharp peaks around zero. A typical image gradient distribution and the fitting results of SGP and three parametric models are shown in Figure 1: the empirical density curve falls at a decreasing rate when moving away from zero, resulting heavy tails that are captured by both hyper-Laplacian and SGP. Given enough independently drawn samples, ω, γ can be numerically estimated using *maximum likelihood* [16].

We test the fitting abilities of Gaussian, Laplacian, hyper-Laplacian and our SGP model on 100 images randomly selected from van Hateren's data set [20]. For each image, we collect the marginal distributions of 6 band-pass filter responses: the gradient components along the horizontal and the vertical directions, and 4 sub-band signals extracted from the steerable pyramid coefficients [21]. We fit these distributions with four models using MLE. The log-likelihood scores of the data are used to measure the model performance. The average log-likelihood scores over the 100 images are presented in Table 1. For each of the six filter responses, SGP and hyper-Laplacian show close fitting scores, outperforming Gaussian and Laplacian with clear numerical advantages.

3. NON-BLIND IMAGE RESTORATION WITH SGP

We denote $\mathbf{x}$ as the original image vector and $\mathbf{y} = \mathbf{x} \otimes \mathbf{k} + \mathbf{n}$ as the observed image degraded by the blurring kernel $\mathbf{k}$ and the additive Gaussian noise $\mathbf{n}$. The problem of non-blind restoration is to reconstruct $\mathbf{x}$ from $\mathbf{y}$ with known $\mathbf{k}, \mathbf{n}$. Given

Filter Response	G	L	h-L	SGP
Gradient-X	1.794	2.181	2.317	**2.342**
Gradient-Y	1.776	2.175	2.288	**2.346**
Sub-band 1	2.661	3.033	**3.183**	3.177
Sub-band 2	1.777	2.113	2.254	**2.258**
Sub-band 3	1.021	1.319	**1.444**	1.442
Sub-band 4	0.360	0.597	0.680	**0.681**

Table 1: The average log-likelihood scores of the four parametric models when fitted to the marginal distributions of the gradients and four band-pass filter responses on van Hateren's data set. The highest log-likelihood scores are marked in bold. Sub-band signals $1-4$ are extracted from the the steerable pyramid coefficients [21]: Sub-band 1 - scale 1, orientation $0°$, Sub-band 2 - scale 2, orientation $45°$, Sub-band 3 - scale 3, orientation $90°$, Sub-band 4 - scale 4, orientation $135°$. G - Guassian, L - Laplacian, h-L: hyper-Laplacian.

the ill-posed nature of the task, we regularize this problem with image priors. Specifically, we employ 2 gradient filters $f_1 = [1, -1], f_2 = [1, -1]^T$, and enforce the sparsity of the filter outputs $\mathbf{x} \otimes f_j$ $(j = 1, 2)$ with the SGP model. By seeking the Bayesian MAP estimation of $\mathbf{x}$, we can convert the restoration task into the following minimization problem:

$$\min_{\mathbf{x}} \sum_i \left(\frac{\lambda}{2}(\mathbf{x} \otimes \mathbf{k} - \mathbf{y})_i^2 + \sum_{j=1}^{2} \log(|\mathbf{x} \otimes f_j|_i + \gamma) \right) \quad (2)$$

where i is the pixel index, and parameter λ balances the contributions of the fidelity term and the sparsity regularizers. Our sparsity regularizer differs from the log prior (studied in [22]) in that our regularizer has a parameter γ from the SGP model, which allows more flexible control on the sparsity of the filter responses. Our solution is also significantly different from the variational method proposed in [22].

This problem poses several challenges for a direct numerical solution: the logarithmic sparsity terms are non-differentiable at zero and involve filtering operations on the unknown $\mathbf{x}$. Following the half-quadratic splitting method [13, 18, 23], we solve this optimization problem by introducing two sets of auxiliary variables $\mathbf{z}_1, \mathbf{z}_2$ at each pixel to decouple the filter responses from the logarithmic penalty terms, resulting the following minimization problem:

$$\begin{aligned} \min_{\mathbf{x},\mathbf{z}_1,\mathbf{z}_2} \sum_i \Big(& \frac{\lambda}{2}(\mathbf{x} \otimes \mathbf{k} - \mathbf{y})_i^2 + \sum_i \sum_{j=1}^{2} \frac{\beta}{2}(\mathbf{x} \otimes f_j - \mathbf{z}_j)_i^2 \\ & + \sum_i \sum_{j=1}^{2} \log(|\mathbf{z}_j|_i + \gamma) \end{aligned} \quad (3)$$

where β is a parameter that increases in an iterative optimization process. When β approaches infinity, the problem defined in Equation (3) converges to the original problem. For

Kernel	Avg. PSNR (in dB)											
	$\sigma_n^2 = 0.0001$				$\sigma_n^2 = 0.001$				$\sigma_n^2 = 0.01$			
	L1	LUT	GISA	SGP	L1	LUT	GISA	SGP	L1	LUT	GISA	SGP
13×13	$\mathbf{25.87}_1$	25.63_4	25.64_2	25.63_3	$\mathbf{24.95}_1$	24.59_4	24.61_3	24.61_2	$\mathbf{23.57}_1$	23.10_4	23.12_3	23.17_2
17×17	$\mathbf{24.35}_1$	24.07_4	24.08_3	24.08_2	$\mathbf{23.61}_1$	23.28_4	23.29_3	23.32_2	$\mathbf{22.64}_1$	22.26_4	22.27_3	22.33_2
21×21	$\mathbf{23.25}_1$	23.04_4	23.05_3	23.07_2	$\mathbf{22.74}_1$	22.50_4	22.51_3	22.53_2	$\mathbf{22.04}_1$	21.67_4	21.69_3	21.75_2
25×25	$\mathbf{22.58}_1$	22.40_4	22.41_3	22.42_2	$\mathbf{22.17}_1$	21.93_4	21.94_3	21.97_2	$\mathbf{21.54}_1$	21.19_4	21.20_3	21.27_2

Table 2: The PSNR results of the four non-blind image restoration methods (L1, LUT, GISA and SGP) on the standard image data set. The reference images are degraded with 4 Gaussian kernels and 3 additive Gaussian noises. The restoration quality of each method is evaluated by the average PSNR value of the image data set. The highest average PSNR values are marked in bold. The subscripts denote the relative rankings of the methods for the specified kernel-noise setting.

Kernel	Avg. PSNR (in dB)											
	$\sigma_n^2 = 0.0001$				$\sigma_n^2 = 0.001$				$\sigma_n^2 = 0.01$			
	L1	LUT	GISA	SGP	L1	LUT	GISA	SGP	L1	LUT	GISA	SGP
15×15	28.62_4	30.01_2	29.99_3	$\mathbf{30.01}_1$	25.17_4	27.01_2	26.99_3	$\mathbf{27.04}_1$	23.25_4	24.60_3	24.62_2	$\mathbf{24.64}_1$
17×17	27.82_4	$\mathbf{29.22}_1$	29.21_2	29.15_3	23.87_4	25.82_2	25.79_3	$\mathbf{25.84}_1$	21.68_4	23.46_2	23.45_3	$\mathbf{23.54}_1$
19×19	28.22_4	$\mathbf{29.57}_1$	29.55_2	29.47_3	23.75_4	25.85_2	25.80_3	$\mathbf{25.90}_1$	21.04_4	23.44_2	23.38_3	$\mathbf{23.64}_1$
21×21	28.89_4	30.40_2	30.36_3	$\mathbf{30.42}_1$	24.86_4	27.01_2	26.96_3	$\mathbf{27.08}_1$	21.87_4	24.07_2	24.04_3	$\mathbf{24.19}_1$
23×23	28.48_4	29.52_2	29.50_3	$\mathbf{29.53}_1$	25.35_4	$\mathbf{26.81}_1$	26.80_3	26.80_2	22.37_4	23.62_3	23.64_2	$\mathbf{23.66}_1$
27×27	26.26_4	$\mathbf{27.53}_1$	27.51_2	27.48_3	23.32_4	25.05_2	25.03_3	$\mathbf{25.06}_1$	21.29_4	22.63_3	22.64_2	$\mathbf{22.71}_1$

Table 3: The PSNR results of the four non-blind image restoration methods (L1, LUT, GISA and SGP) on the standard image data set. The reference images are degraded with 6 motion-blur kernels from [3] and 3 additive Gaussian noises. The restoration quality of each method is evaluated by the average PSNR value of the image data set. The highest average PSNR values are marked in bold. The subscripts denote the relative rankings of the methods for the specified kernel-noise setting.

a fixed β, the above problem can be decomposed into two subproblems with alternative minimization.

Given fixed $\mathbf{z}_1, \mathbf{z}_2$, we first minimize the $\mathbf{x}$ subproblem:

$$\min_{\mathbf{x}} \sum_i \left(\frac{\lambda}{2} (\mathbf{x} \otimes \mathbf{k} - \mathbf{y})_i^2 + \sum_{j=1}^{2} \frac{\beta}{2} (\mathbf{x} \otimes f_j - \mathbf{z}_j)_i^2 \right) \quad (4)$$

Under the periodic boundary condition, this subproblem can be efficiently solved in closed-form with FFT and inverse FFT. Details about this subproblem can be found in [18].

Given fixed $\mathbf{x}$, We optimize $\mathbf{z}_1, \mathbf{z}_2$ independently:

$$\min_{\mathbf{z}_j} \sum_i \left(\frac{\beta}{2} (\mathbf{x} \otimes f_1 - \mathbf{z}_j)_i^2 + \log(|\mathbf{z}_j|_i + \gamma) \right) \quad j = 1, 2 \quad (5)$$

which can be further converted into a common 1D minimization problem on each pixel i:

$$\min_z g(z) = \frac{\beta}{2} (z - v)^2 + \log(|z| + \gamma) \quad (6)$$

where $v = (\mathbf{x} \otimes f_1)_i$ or $(\mathbf{x} \otimes f_2)_i$. An important property about $g(z)$ is that $g'(z) = 0$ can be turned into a quadratic equation, which allows one to compute the roots with analytic formulae and find the global minimum of $g(z)$ efficiently.

Our solution varies with the parameter settings of β and γ. If $\gamma > \sqrt{\frac{1}{\beta}}$, the optimal z^* is computed as follows:

$$z^* = \begin{cases} \text{sgn}(v) \cdot z_{root}(|v|, \beta, \gamma), & |v| \geq \frac{1}{\gamma\beta} \\ 0, & |v| < \frac{1}{\gamma\beta} \end{cases} \quad (7)$$

where sgn is the signum function, and z_{root} is the larger root of the equation $g'(z) = 0$:

$$z_{root}(|v|, \beta, \gamma) = \frac{1}{2}(|v| - \gamma) + \frac{1}{2}\sqrt{(|v| + \gamma)^2 - \frac{4}{\beta}} \quad (8)$$

If $\gamma \leq \sqrt{\frac{1}{\beta}}$, z^* is summarized as follows:

$$z^* = \begin{cases} \text{sgn}(v) \cdot z_{root}, & |v| \geq \frac{1}{\gamma\beta} \\ \underset{z \in \{0, \text{sgn}(v) \cdot z_{root}\}}{\text{argmin}} g(z), & 2\sqrt{\frac{1}{\beta}} - \gamma \leq |v| < \frac{1}{\gamma\beta} \\ 0, & |v| < 2\sqrt{\frac{1}{\beta}} - \gamma \end{cases} \quad (9)$$

Derivation details will be given in an extended report. Both solutions are in the form of nonlinear shrinkage operations on v with different threshold values. Compared to the solutions of hyper-Laplacian [13, 14], SGP is conceptually more favorable, since z^* can be computed directly without resorting to look-up tables or iterative approximations.

4. EXPERIMENTAL RESULTS

We evaluate the restoration performance of our method (denoted as SGP), as well as three state-of-the-art methods that rely on gradient-based priors: the fast TV method (denoted as L1) [18], a method based on the hyper-Laplcian prior and look-up tables (denoted as LUT) [13], and a recent hyper-Laplacian method based on general iterative shrinkage (denoted as GISA) [14].

Original Image Corrupted, 16.61dB L1, 20.74dB LUT, 21.96dB GISA, 21.96dB SGP, 22.06dB

Fig. 2: The restoration results of the 'barbara' example. The original clean image is severely degraded by a large 27×27 motion-blur kernel and noise $\sigma_n^2 = 10^{-2}$. Details are best viewed in the electronic version.

We test all four methods on a standard image data set, containing 12 grayscale images [24]. All images are of size 512×512. We create the degraded images with various kernels and noise levels: 4 Gaussian kernels with standard deviations $6.5, 8.5, 10.5, 12.5$ (size ranging from 13×13 to 25×25), 6 motion blur kernels recovered from the real-world images (size ranging from 15×15 to 27×27) [3]. For the additive gaussian noise, we use 3 noise levels with increasing variances $\sigma_n^2 = 0.0001, 0.001, 0.01$.

The four methods are implemented within the same framework, with a regularization parameter λ and a model-related parameter: for LUT and GISA, a parameter $\alpha \in (0, 1)$ controls the sparseness of the gradients; for SGP, we have a γ parameter with the similar purpose; the L1 method needs no extra parameters. We use a common λ value for all the methods, which varies between different noise levels. For noise variances $\sigma^2 = 0.0001, 0.001, 0.01$, we experimentally set $\lambda = 2000, 350, 60$. LUT and GISA use $\alpha = 0.7$, while the γ value of SGP is fixed to 0.4 for the best possible overall performance. The quantitative results are measured with the Peak Signal-to-Noise Ratio (PSNR) values.

Results with Gaussian Kernels The average PSNR values of the four methods with Gaussian kernels and three noise levels are presented in Table 2. Surprisingly, we find that the L1 method consistently outperforms the other three methods for all kernel-noise settings. Our SGP method outperforms GISA and LUT for all but one of the cases, while GISA and LUT produce very close results.

Results with Motion-Blur Kernels The PSNR results with the motion-blur kernels from [3] and various noise levels are presented in Table 3. For these moving-path related kernels, the L1 method performs worst for all the testing cases. For the small noise level ($\sigma_n^2 = 10^{-4}$), LUT, GISA and SGP showed some mixed performance: for some kernels, LUT gives the best results, while for some other kernels, SGP performs better than LUT and GISA. Overall, the results of the three methods are quite close to each other. However, with increasing noise levels, SGP outperforms the other three methods for most cases. We provide an example in Figure 2:

Steps	Average Running Time (in Seconds)			
	L1	LUT	GISA	SGP
Full	**0.591**	1.058 (offline) 0.624 (online)	0.599	**0.591**
$\mathbf{x}$-step	0.576			
$\mathbf{z}$-step	**0.014**	0.048	0.023	**0.014**

Table 4: Average running time (in seconds) of L1, LUT, GISA and SGP on the standard image data set.

for this severely degraded image, our method can still recover the main image structures, with fewer artifacts (see the noisy speckles) than LUT and GISA.

Running Time The average running time of the four methods are presented in Table 4. Our method runs as fast as the L1 method, slightly faster than GISA and LUT. LUT requires some extra computation efforts to build the look-up tables in an offline process. Note that all four methods solve exactly the same $\mathbf{x}$ subproblem, which dominates the running time with FFT operations. For the $\mathbf{z}$ subproblem, SGP is about $1.64\times$ faster than GISA in our implementation.

5. CONCLUSIONS

We have presented a non-blind image restoration method based on the symmetric generalized pareto model, which shows competitive performance in restoration quality and processing speed. As future work, we would like to employ the SGP priors in synthesis-based image models [25]. We also found that performance of some restoration algorithms has a strong dependence on the form of the kernels. It would be of interest to further investigate the exact effect of kernel characteristics on the restoration techniques.

Acknowledgement

This work is partially funded by National Natural Science Foundation of China (Grant No. 61271430, 61172104, and 61332017).

6. REFERENCES

[1] M. R. Banham and A. K. Katsaggelos, "Digital image restoration," *IEEE Signal Processing Magazine*, vol. 14, no. 2, pp. 24–41, 1997.

[2] D. Krishnan, T. Tay, and R. Fergus, "Blind deconvolution using a normalized sparsity measure," in *CVPR*, 2011, pp. 233–240.

[3] A. Levin, Y. Weiss, F. Durand, and W. T. Freeman, "Understanding and evaluating blind deconvolution algorithms," in *CVPR*, 2009, pp. 1964–1971.

[4] J. Portilla, V. Strela, M. J. Wainwright, and E. P. Simoncelli, "Image denoising using scale mixtures of Gaussians in the wavelet domain," *IEEE Trans. Image Process.*, vol. 12, pp. 1338–1351, 2003.

[5] S. Roth and M. Balck, "Field of experts," *Int. J. Comput. Vision*, vol. 82, no. 2, pp. 205–229, 2009.

[6] D. Zoran and Y. Weiss, "From learning models of natural image patches to whole image restoration," in *ICCV*, 2011, pp. 479–486.

[7] D. Field, "What is the goal of sensory coding?," *Neural Computation*, vol. 6, no. 4, pp. 559–601, 1994.

[8] J. Huang and D. Mumford, "Statistics of natural images and models," in *CVPR*, 1999, pp. 1541–1547.

[9] E. Simoncelli and E. Adelson, "Noise removal via Bayesian wavelet coring," in *ICIP*, 1996, vol. 1, pp. 379–382.

[10] M. J. Wainwright and E. Simoncelli, "Scale mixtures of Gaussians and the statistics of natural images," in *NIPS*, 2000, vol. 12, pp. 855–861.

[11] A. Levin, R. Fergus, F. Durand, and W. T. Freeman, "Image and depth from a conventional camera with a coded aperture," *ACM Trans. Graph.*, vol. 26, no. 3, 2007.

[12] A. Levin and Y. Weiss, "User assisted separation of reflections from a single image using a sparsity prior," *IEEE Trans. Pattern Anal. Mach. Intell.*, vol. 29, no. 9, pp. 1647–1654, 2007.

[13] D. Krishnan and R. Fergus, "Fast image deconvolution using hyper-Laplacian priors," in *NIPS*, 2009, pp. 1033–1041.

[14] W. Zuo, D. Meng, L. Zhang, X. Feng, and D. Zhang, "A generalized iterated shrinkage algorithm for non-convex sparse coding," in *ICCV*, 2013, pp. 217–224.

[15] P. Garrigues and B. A. Olshausen, "Group sparse coding with a Laplacian scale mixture prior," in *NIPS*, 2010, pp. 676–684.

[16] Y. Jia and T. Darrell, "Heavy-tailed distances for gradient based image descriptors," in *NIPS*, 2011, pp. 397–405.

[17] A. Armagan, D. Dunson, and J. Lee, "Generalized double pareto shrinkage," *Statistica Sinica*, vol. 23, pp. 119–143, 2013.

[18] Y. Wang, J. Yang, W. Yin, and Y. Zhang, "A new alternating minimization algorithm for total variation image reconstruction," *SIAM Journal on Imaging Sciences*, vol. 1, no. 3, pp. 248–272, 2008.

[19] J. Pickands, "Statistical inference using extreme order statistics," *The Annals of Statistics*, vol. 3, no. 1, pp. 119–131, 1975.

[20] J. H. van Hateren and A. van der Schaaf, "Independent component filters of natural images compared with simple cells in primary visual cortex," *Proceedings: Biological Sciences*, vol. 265, no. 1394, pp. 359–366, 1998.

[21] E. P. Simoncelli and W. T. Freeman, "The steerable pyramid: A flexible architecture for multi-scale derivative computation," in *ICIP*, 1995, vol. 3, pp. 444–447.

[22] S. D. Babacan, R. Molina, M. N. Do, and A. K. Katsaggelos, "Bayesian blind deconvolution with general sparse image priors," in *ECCV*, 2012.

[23] D. Geman and C. Yang, "Nonlinear image recovery with half-quadratic regularization," *IEEE Trans. Image Process.*, vol. 4, no. 7, pp. 932–946, 1995.

[24] K. Dabov, A. Foi, V. Katkovnik, and K. Egiazarian, "Image denoising by sparse 3d transform-domain collaborative filtering," *IEEE Trans. Image Process.*, vol. 16, no. 8, pp. 2080–2095, 2007.

[25] M. Elad, P. Milanfar, and R. Rubinstein, "Analysis vs synthesis in signal priors," *Inverse Problems*, vol. 23, no. 3, pp. 947–968, 2007.